Nonequilibrium athermal random-field Ising model on hexagonal lattices

Svetislav Mijatović,[1] Dragutin Jovković,[2,*] and Djordje Spasojević[1]
[1]*Faculty of Physics, University of Belgrade, P.O.B. 44, 11001 Belgrade, Serbia*
[2]*Faculty of Mining and Geology, University of Belgrade, P.O.B. 162, 11000 Belgrade, Serbia*

(Received 27 July 2020; revised 12 January 2021; accepted 8 March 2021; published 25 March 2021)

We present the results of a study providing numerical evidence for the absence of critical behavior of the nonequilibrium athermal random-field Ising model in adiabatic regime on the hexagonal two-dimensional lattice. The results are obtained on the systems containing up to 32 768 × 32 768 spins and are the averages of up to 1700 runs with different random-field configurations per each value of disorder. We analyzed regular systems as well as the systems with different preset conditions to capture behavior in thermodynamic limit. The superficial insight to the avalanche propagation in this type of lattice is given as a stimulus for further research on the topic of avalanche evolution. With obtained data we may conclude that there is no critical behavior of random-field Ising model on hexagonal lattice which is a result that differs from the ones found for the square and for the triangular lattices supporting the recent conjecture that the number of nearest neighbors affects the model criticality.

DOI: 10.1103/PhysRevE.103.032147

I. INTRODUCTION

Systems and materials whose response to external driving is realized in a train of avalanches manifesting power-law distributions are becoming more extensively studied in recent decades. This type of behavior, present in a vast variety of systems (e.g., earthquakes [1–3], neural networks [4], martensitic transformations [5], motion in granular materials [6], etc.), stimulated the advent of several theoretical models, including those referencing the systems whose behavior is dominated by some intrinsic disorder [7].

Among these models [8–13], a prominent role is played by the random-field Ising model (RFIM) [14] and in particular by its nonequilibrium athermal version [15] describing the hard ferromagnetic materials with quenched disorder. In this version, the time evolution is monitored while the studied system, responding to a variation of the external magnetic field by following local dynamical rules, traverses the nonequilibrium states which causes emanation of the Barkhausen noise [16,17].

In numerous studies of the nonequilibrium athermal RFIM many aspects of its behavior have been revealed, see [18] for a review. Most importantly, it was shown that on hypercubic lattices for dimensions $d \geqslant 6$ the model can be described in the mean field approximation, see [19] for instance. In addition $2 \leqslant d \leqslant 5$ there is a nontrivial phase transition from ferromagnetic to paramagnetic phase at some critical value of disorder R_c [20–25], which turned out to be different from the corresponding transition in equilibrium athermal RFIM [26] treating the least energy states as a function of the applied external field. In Ref. [27] the authors perform simulations on two-dimensional Voronoi lattice that prevent the effects of faceting, for a wide range of disorders, and derive invariant scaling combinations using normal form theory of the renormalization group that eventually serve to determine the arguments of the universal scaling function necessary to perform scaling collapses. They found that the critical disorder in such system is zero. However, this result refers to only one type of two-dimensional lattice and it is not clear how it can be extended to every two-dimensional lattice. Lately, a progress in equilibrium version of RFIM presented important answers on the universality principles [28,29], dimensional reduction [30] and supersymmetry [31] of the model.

A question of the nonequilibrium athermal RFIM behavior on lattices of the same local type but changing dimensions was raised in papers [32–36] and discovered that there is analytic dependence of critical values of model parameters on continuously changing lattice dimension.

Within the course of these discoveries, a standpoint gradually emerged that the universality classes, characterizing the criticality of the nonequilibrium athermal model, are determined only by the dimensionality of the underlying lattice like in the equilibrium model. Recently, a group of authors challenged this opinion by putting forward a competitive conjecture that the universality classes in nonequilibrium model are determined by the topology of the lattice rather than by the lattice dimensionality [37–40]. This implies that the number of nearest neighbors (i.e., coordination number) and the way how these neighbors are connected influence the universality classes which was to some extent confirmed in Ref. [41] by comparing the criticality of the model on the triangular and quadratic lattices that are both embedded in two-dimensional (2D) space, but have different numbers of the nearest neighbors (six and four, respectively).

We address here the foregoing conjecture by putting forward the results of our numerical study of the behavior of the nonequilibrium athermal RFIM placed on the hexagonal (i.e., honeycomb) 2D lattice where each spin has three nearest

[*]Also at the Faculty of Physics, University of Belgrade, P.O.B. 44, 11001 Belgrade, Serbia.

neighbors. We provide numerical evidence that under adiabatic driving by the external magnetic field this model does not exhibits a nontrivial critical behavior. Compared with the behavior of the model on the square and on the triangular lattices, on the hexagonal lattice there will be no ferromagnetic phase for any nonzero disorder making questionable the existence of a single universality class for all periodic (i.e., translationally invariant) 2D lattices in the case of nonequilibrium athermal RFIM.

The paper is organized as follows. In Sec. II we give the explanation of the nonequilibrium athermal RFIM along with its numerical implementation, emphasizing all points relevant for this paper. Section III contains results on avalanche parameters distributions and their collapses that may be obtained for a nonunique set of parameters and exponents. Section IV presents the data gathered on systems with preset initial conditions that mimic the behavior in thermodynamic limit. In Sec. V are shown results on avalanche propagation, giving a closer insight of how an avalanche evolves throughout the hexagonal lattice. Last, in Sec. VI we discuss the results and give the conclusion of the paper.

II. MODEL

The athermal random-field Ising model treats a system of N classical Ising spins $\{s_i = \pm 1\}_{i=1}^{N}$ with no thermal fluctuations. The spins are located at sites i of some underlying lattice, and the nearest-neighbor spins are ferromagnetically coupled. Besides, each spin s_i interacts with the external homogeneous magnetic field H and also with a magnetic field h generated by quenched impurities whose local values h_i vary randomly from site to site. So, the Hamiltonian of such spin system can be taken as

$$\mathcal{H} = -J \sum_{\langle i,j \rangle} s_i s_j - H \sum_i s_i - \sum_i h_i s_i \,, \tag{1}$$

where $J > 0$ is the strength of ferromagnetic coupling (in this paper $J = 1$) and the summation in the first term is done over all distinct (unordered) pairs of nearest neighbors $\langle i, j \rangle$. The second sum in Eq. (1) describes the interaction between the spins and the external magnetic field H, while in the third sum, $h_i s_i$ stands for the interaction of spin s_i with the random-field h having local value h_i at the spin's site. Therefore, the effective (i.e., total) magnetic field that acts on the spin s_i is

$$h_i^{\text{eff}} \equiv \sum_j s_j + H + h_i \,, \tag{2}$$

where the summing is done over all nearest neighbors s_j of the spin s_i. The local values h_i of the random field are chosen from some zero-mean probability distribution, here the Gaussian distribution $\rho(h) = e^{-h^2/2R^2}/\sqrt{2\pi}R$ with zero mean and standard deviation R, which is the most important model parameter, called disorder. These local values are chosen independently at different lattice sites, giving $\langle h_i h_j \rangle = R^2 \delta_{i,j}$, where $\delta_{i,j}$ is the Kronecker-δ function and $\langle \ldots \rangle$ means averaging over all different configurations of random fields. Any distribution that satisfies previous conditions may be chosen as distribution $\rho(h)$. The reason we choose Gaussian distribution is because in the past studies of RFIM it was the most common choice of random-field distribution and to adequately compare present results to the some previous we should stick to the same choice of random-field distribution. However, further analysis on different random-field distributions would be useful for better understanding of nonequilibrium RFIM behavior.

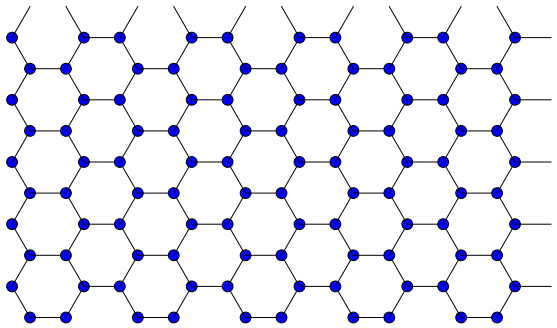

FIG. 1. Hexagonal lattice in two dimensions. Each site of this lattice has three nearest neighbors. The lattice is shown to avoid possible confusion with its dual triangular lattice with six nearest neighbors for each site.

In the nonequilibrium model the system's dynamics is governed by the local (and deterministic) dynamical rule stating that a spin is stable if is aligned with the effective magnetic field h_i^{eff} at its site; otherwise, the spin is unstable and flips at the next moment of (discrete) time decreasing, thus, the system's energy. This spin flipping may destabilize some of its neighbors causing the unstable spins to flip, which in turn will destabilize their neighbors, and in this way, an avalanche of spin flipping is created. The avalanche lasts as long as there are unstable spins, and dies when all spins become stable at the current value of the external field. In a consequence, the energy of such metastable states, like for the real ferromagnets driven by an external field, does not necessarily attain its global minimum for the corresponding external field, and this makes the main difference between the nonequilibrium and equilibrium model (in which all traversed states are global energy minima).

After avalanches die, the system can be destabilized only by changing the external field. Of a particular theoretical importance is the so-called adiabatic regime as the zero limit case of the finite driving rate encountered in experiments. In this regime the external field remains constant during the avalanches and, instead of being infinitely slowly varied between the avalanches (say, increased), the external field is changed exactly by the amount that flips only the least stable spin. Under such driving at most one avalanche is active at a time, and the simulation speed is greatly increased.

In this paper, we analyze the nonequilibrium behavior in the adiabatic regime of the athermal RFIM spin systems situated at a hexagonal lattice in two dimensions, see Fig. 1. All spins at this lattice have three nearest neighbors. Initially, we set the external field to $H = -\infty$ and all spins to -1 (unless stated otherwise), and then we increase the field until all spins are being flipped. Each avalanche starts at the moment $t = 1$ of discrete time when only one spin flips, making its neighbors potentially unstable. After that, at $t = 2$, all unstable spins from $t = 1$ flip, making their neighbors potentially unstable and so on. The sum of all flipped spins

during one avalanche represents the avalanche-size S, and the number of discrete time steps during the avalanche represents its duration, T. With this choice of system evolution, and using periodic boundary conditions, we repeat the simulations for many different configurations of the random field and subsequently analyze the system response averaged over all employed configurations.

During an active avalanche we track all the nearest neighbors of the spins flipped at the moment t. We check if they are unstable and flip them in the moment $t+1$ in case they are unstable. This is a relatively fast process. The most time-consuming process in these simulations is the process of finding the next spin to flip once the avalanche is over (i.e., the first spin in the following avalanche). Brute force algorithm would suggest to check all nonflipped spins in the system and to see which one has the lowest effective field acting on it. In big systems such as $32\,768 \times 32\,768$ the time needed for such approach is extremely large. To decrease the time consumption by the process of finding the first flipped spin in an avalanche we used the sorted list algorithm which we implemented in Fortran. This algorithm is described in Ref. [42] and even in more details in Ref. [43].

Results gathered from simulations are analyzed using the programs coded in Fortran, Visual Basic and Wolfram Mathematica. We used Fortran and Visual Basic to obtain statistics regarding the avalanche parameters as well as magnetization and susceptibility. On the other side, we used Wolfram Mathematica and its implemented functions to obtain the fitting and collapse procedures to the desired accuracy.

III. REGULAR SYSTEMS

We present the results regarding the behavior of the nonequilibrium athermal RFIM spin systems situated at hexagonal lattices in two dimensions for regular systems. In this paper by regular systems we mean the systems whose all spins are pointing downwards in the beginning of the simulation and are free to evolve. Such systems are adiabatically driven by the external magnetic field along the entire rising part of the magnetization curve and the final results are the quenched averages over different configurations of the random field obtained in 200 runs for each disorder on the lattice having $32\,768 \times 32\,768$ spins and closed boundary conditions. For the sake of better precision, this number of runs is increased to 1700 in the determination of the effective critical disorder done for systems with sizes ranging from 256×256 to $32\,768 \times 32\,768$.

A. Critical behavior

Without thermal fluctuations, the behavior of the RFIM spin system in adiabatic regime is governed by disorder R and system size L. If the model exhibits a nontrivial critical behavior then there is a critical value of disorder R_c such that for $R > R_c$ the magnetization curves $M_R(H)$ of infinite systems are smooth functions of external field H, while for $R < R_c$ these curves have a jump at the effective critical value $H_c^{\rm eff}(R)$ of the external magnetic field. When $R \to R_c$, the magnetization curves from both families tend to the critical magnetization curve which corresponds to $R = R_c$. Like

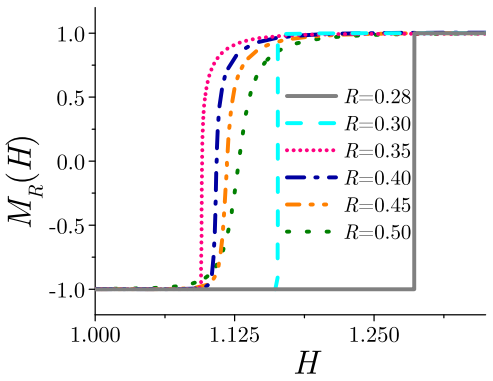

FIG. 2. Examples of magnetization curves obtained in a single run for the values of disorder in range $R = 0.28$–0.50 on the system having $32\,768 \times 32\,768$ spins.

for $R > R_c$ curves, this critical curve is still a continuously differentiable function of H, except at the critical external field $H_c = \lim_{R \to R_c} H_c^{\rm eff}(R)$ where its first derivative dM/dH is infinite and magnetization reaches the critical value $M_c = M_{R_c}(H_c)$.

In Fig. 2, we show a set of magnetization curves obtained in the range 0.28–0.50 of disorder R at the $32\,768 \times 32\,768$ lattice. Each curve is acquired in a single run for given disorder. However, there are some important differences manifested here, and also in comparison of the magnetization curves of infinite systems and finite RFIM systems in general. Thus, the jumps of magnetization encountered in single runs of finite systems are caused not by the (obviously impossible) infinite avalanches but by large avalanches spanning the finite system along at least one of its spatial dimensions. These spanning avalanches are likely to appear below the so-called effective critical disorder $R_c^{\rm eff}(L)$ that depends on the lattice size L and for the model at hexagonal lattice at most one spanning avalanche is found in a single run like on quadratic and triangular 2D lattices, see Refs. [41,44] and also Refs. [33,45,46]. As the size of that spanning avalanche and the value of the external magnetic field at which this avalanche is triggered both depend on the configuration of the quenched random field, the averaged magnetization curves acquired above $R_c^{\rm eff}(L)$ have no jump but instead exhibit finite slope everywhere like on quadratic 2D lattice, see Ref. [44] for details.

The effective critical field $H_c^{\rm eff}(R)$ is determined as the value of external magnetic field for which system susceptibility attains its maximum. Note that the effective critical field depends on system size L as well, but we omit that for the simpler notation. We define the susceptibility $\chi_R(H)$ as the change in magnetization for a given external field, $\chi_R(H) = dM/dH$ [47,48], i.e., twice the number of flipped spins at external field H (since one flipped spin changes magnetization by value 2) divided by the number of spins in the system. In the main panel of Fig. 3(a) is presented one example of the susceptibility curve averaged over 200 runs for disorder $R = 0.5$ and lattice size $L = 32\,768$. In the upper left and upper right insets of Fig. 3(a) are presented the susceptibility curves for two single runs (two different random-field configurations) for each of the disorders $R = 0.15$ and $R = 0.55$, respectively, and lattice size

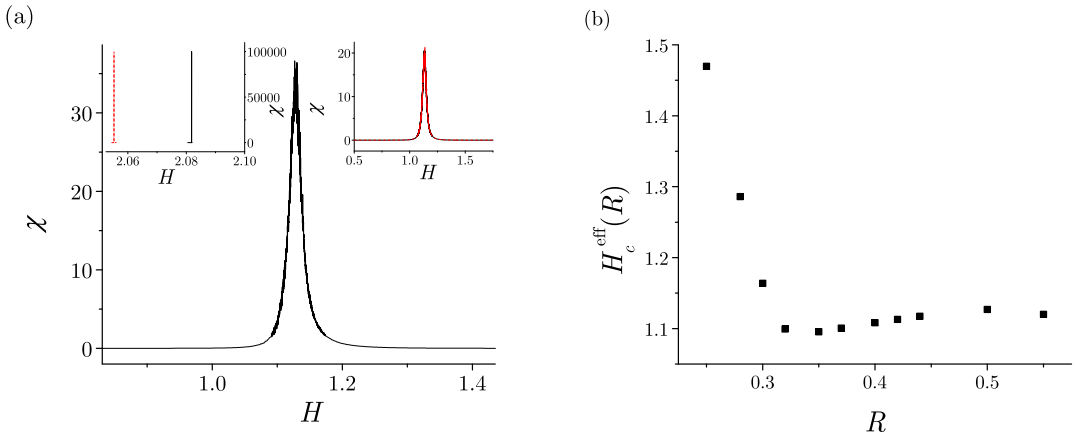

FIG. 3. (a) Main panel: Susceptibility curve of 32 768 × 32 768 system and disorder $R = 0.5$, averaged over 200 runs. Upper left inset: two single-run susceptibility curves, black solid and red dashed curve, for systems of size 32 768 × 32 768 and disorder $R = 0.15$. Upper right inset: two single-run susceptibility curves, black solid and red dashed curve, almost overlapped for the 32 768 × 32 768 system and disorder $R = 0.55$. (b) The effective critical field $H_c^{\rm eff}$ versus disorder R (for the 32 768 × 32 768 system).

32 768 × 32 768. We see that for disorders that are below the effective critical disorder, see Sec. III A 1, the single-run susceptibility curves differ a lot, meaning that a large number of runs is needed to obtain sufficiently smooth averaged susceptibility curve and effective critical field. However, when disorder is above the effective critical disorder there are no much fluctuations in sample-to-sample curves so obtaining of a smooth susceptibility curve is possible in a smaller number of runs. In Fig. 3(b) are presented the effective critical fields for system of size 32 768 × 32 768 and various disorders.

1. Effective critical disorder

For the systems of finite-size L, the effective critical disorder $R_c^{\rm eff}(L)$ can be found from the curve showing the number N_2 of 2D spanning avalanches (i.e., avalanches spanning the system along both of its spatial dimensions) as a function of disorder R. This is illustrated in Fig. 4 by the N_2 data (pink dots), obtained in the range of disorder 0.24 to 0.46 in the case of system having 5792 × 5792 spins. Like in the cases of quadratic and triangular 2D lattices [41,44], and also for the modified 2D spanning avalanches in the case of (thin) cubic 3D lattices [33], these data can be fitted by the two-parameter model function

$$N_{R_0,W}(R) = 0.5 \times \mathrm{erfc}[(R - R_0)/W]\,, \tag{3}$$

plotted by the full line; $\mathrm{erfc}(x) = 2/\sqrt{\pi}\int_x^\infty e^{-t^2}dt$ is the complementary error function. Parameter W of this model function describes the width of the transition region of disorder in which the N_2 data roughly fall from 1 to 0 (more precisely from 0.76025 to 0.23975, see Ref. [33]), while the center R_0 of this transition region can be taken as the effective critical disorder $R_c^{\rm eff}(L)$ for the given lattice size L. The effective critical disorder $R_c^{\rm eff}(L)$ obtained in this way is always greater than the critical disorder, $R_c^{\rm eff}(L) > R_c$, and tends to it in the thermodynamic limit, $\lim_{L\to\infty} R_c^{\rm eff}(L) = R_c$.

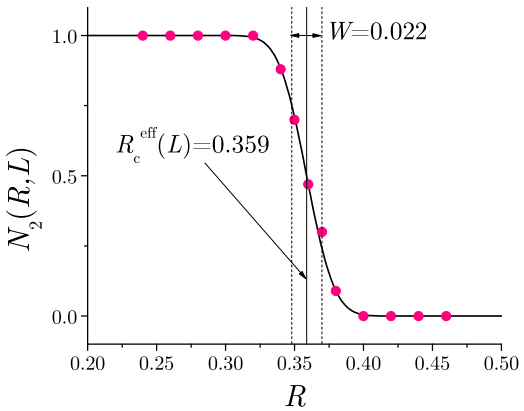

FIG. 4. Number of two-dimensional spanning avalanches per single-run N_2 in the 5792 × 5792 spin system (pink dots) for disorders in the range $R = 0.24$–0.46, together with the fitting curve Eq. (3). 100 simulations employing different random-field configurations were performed for each of these values of disorder.

In Table I we present the values of effective critical disorders for various lattice sizes. For comparison, we show the values of effective critical disorders for other two two-dimensional lattice types (square and triangular). One can try to plot the values of effective critical disorders versus the linear lattice size for hexagonal lattice, analogously as presented in, e.g., Refs. [25,41] for square and triangular lattices, to obtain the value of critical disorder. However, applying this method, it is impossible to obtain R_c with the satisfying accuracy, since it turns out that all values of R_c, from 0 to 0.31, give equally good fitting results. This was not the case for the square or triangular lattices. In inset of Fig. 20 in Ref. [25] is presented how different values of critical disorder for square lattice lead to the obviously different fit qualities. Similarly can be done with the triangular lattice using here presented values of effective critical disorders and results from Ref. [41].

2. Finite-size effects

In Fig. 3(b) the following behavior of $H_c^{\rm eff}(R)$ may be observed. While the disorder is greater than the effective critical disorder, the effective critical field increases as disorder increases, which is expected. However, for $R < R_c^{\rm eff}(L)$ we notice that effective critical field decreases as disorder increases

TABLE I. Effective critical disorders for three lattice types for different systems' size, L ranged from 256 up to 65 536.

L	256	512	1024	2048	8192	16 384	32 768	65 536
Hexagonal	0.421 ± 0.003	0.409 ± 0.003	0.388 ± 0.004	0.381 ± 0.004	0.356 ± 0.005	0.349 ± 0.005	0.341 ± 0.005	0.334 ± 0.005
Square	0.837 ± 0.003	0.798 ± 0.004	0.761 ± 0.004	0.716 ± 0.004	0.669 ± 0.005	0.648 ± 0.005	0.629 ± 0.005	0.614 ± 0.006
Triangular	1.478 ± 0.003	1.369 ± 0.003	1.265 ± 0.004	1.207 ± 0.004	1.107 ± 0.004	1.075 ± 0.005	1.036 ± 0.005	1.010 ± 0.005

and we show here that this happens due to the finite-size effects. To this end let us use the probability $p(S_{NN}, H, R)$ that the spin, whose sum of nearest neighbors is S_{NN}, will flip if the disorder value is R and external field is H:

$$p_{H,R}(S_{NN}) = \int_{-(S_{NN}+H)}^{\infty} \rho(h)dh = \frac{1}{2}\left[1 + \mathrm{erf}\left(\frac{S_{NN}+H}{R\sqrt{2}}\right)\right]. \quad (4)$$

Here, $\mathrm{erf}(x) = 2/\sqrt{\pi}\int_0^x \exp(-t^2)dt$ is the standard error function. In the following text we will denote this flipping probability simply by $p(S_{NN})$.

In Fig. 5 we present by points how H_c^{eff} depends on R for three different values of L ($L = 256$ squares, $L = 1024$ circles, $L = 32\,768$ triangles). For small disorders a linear dependence of $H_c^{\mathrm{eff}}(R)$ is observed and the slope of the linear curve increases with L. This happens because the system is too small for that low value of disorder so that it takes larger external field to even flip the first spin in the system. Once the first spin is flipped the sum of its nearest neighbors becomes -1, instead of -3 before flipping. This, in combination with the external field that is already high enough (high external field was needed to flip the first spin), allows the spanning avalanche to occur. Basically, the values of $H_c^{\mathrm{eff}}(R)$ for lower disorders are determined by the value of the external field needed to flip the first spin in the system. This leads to the conclusion that the linear dependence of $H_c^{\mathrm{eff}}(R)$ can be described by the equation connecting the system size L and the probability $p(-3)$ as $p(-3) = 1/L^2$. This means that the external field should take the value that flips one spin in the system of L^2 spins. Combined with Eq. (4) this equation leads

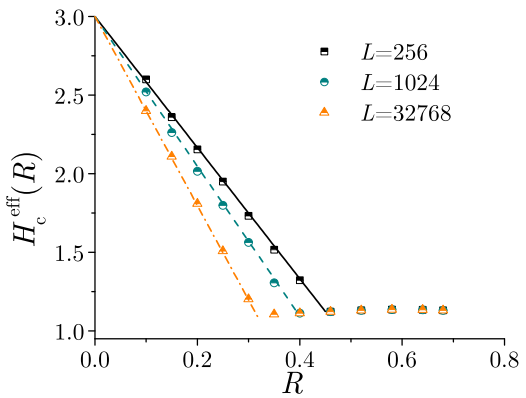

FIG. 5. Effective critical field versus disorder for three different values of system size. For $L = 256$ the effective critical field is presented by black squares, for $L = 1024$ by blue circles, for and $L = 32\,768$ by orange triangles. Straight lines represent the linear dependence given by Eq. (5) which holds for low values of disorder.

to the linear dependence

$$H_c^{\mathrm{eff}}(R) = 3 - R\sqrt{2}\,\mathrm{erf}^{-1}\left(1 - \frac{2}{L^2}\right), \quad (5)$$

between the external critical field and disorder, where $\mathrm{erf}^{-1}(x)$ is the inverse error function. In Fig. 5, Eq. (5) is confirmed by the straight lines which fit the numerical data for $L = 256$ (solid line), $L = 1024$ (dashed line) and $L = 32\,768$ (dash-dotted line) up to the effective critical disorder for the given system size.

B. Distributions

1. Avalanche-size distribution

In infinite systems manifesting a nontrivial critical behavior the distributions of avalanche-size S triggered at the external field H and disorder $R > R_c > 0$ follow the scaling prediction [8,15,24,25]

$$D_{R,H}^{(S)}(S) = S^{-\tau}\mathcal{D}_+^{(S)}(S^\sigma r, h' r^{-\beta\delta}). \quad (6)$$

Here, σ is the cutoff exponent describing the scaling $S_{\max} \sim r^{-1/\sigma}$ of the largest avalanche-size $S_{\max}$ with the reduced disorder $r = 1 - R_c/R$, τ is the avalanche-size exponent, $h' = H - H_c - br$ is a reduced magnetic field rotated by a parameter b, with H_c being the critical external field, β is the critical exponent that describes the scaling of the magnetization jumps below R_c, $\Delta M \sim |r|^\beta$, δ is the critical exponent that describes how reduced magnetization scales with the reduce magnetic field, $[M(H) - M_c] \sim h'^\delta$, with M_c being the critical magnetization and $M(H)$ the magnetization of the system when the external field is equal to H, and $\mathcal{D}_+^{(S)}$ is the corresponding universal scaling function that depends on two variables X, Y taken in Eq. (6) as $X = S^\sigma r$ and $Y = h' r^{-\beta\delta}$. Integrating the distribution $D_{R,H}^{(S)}(S)$ over all values of external field H, one gets the integrated avalanche-size distribution $D_R^{(S,\mathrm{int})}(S) \equiv \int_{-\infty}^{\infty} D_{R,H}^{S}(S)dH$ which scales as

$$D_R^{(S,\mathrm{int})}(S) = S^{-(\tau+\sigma\beta\delta)}\hat{\mathcal{D}}_+^{(S,\mathrm{int})}(S^\sigma r), \quad (7)$$

and has $\hat{\mathcal{D}}_+^{(S,\mathrm{int})}(X) \equiv \int_{-\infty}^{\infty}\mathcal{D}_+^{(S)}(X,Y)dY$ as its universal scaling function. This scaling predicts that if we plot the $D_R^{(S,\mathrm{int})}(S)S^{\tau+\sigma\beta\delta}$ data against $S^\sigma r$ then the integrated size distributions, pertaining to various disorders, should collapse onto a single curve.

Scaling predictions analogous to Eqs. (6) and (7) exist in the case of avalanche-size distributions for finite systems as well. These distributions, collected on sufficiently large finite systems, match the corresponding distributions of infinite systems, and therefore can be collapsed using Eqs. (6) and (7) in what follows.

Instead of distributions of avalanches triggered only at a given value of the external field, whose collecting is obviously

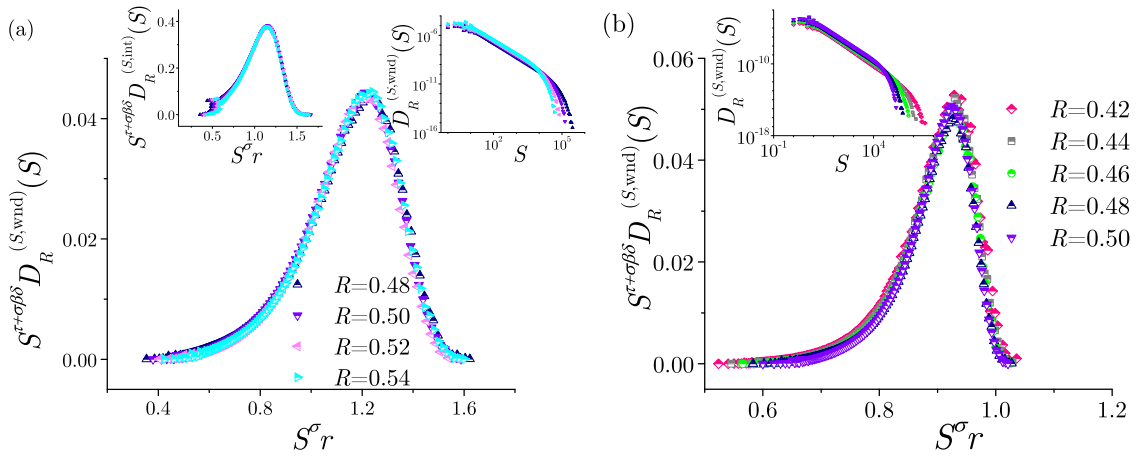

FIG. 6. (a) Upper right inset: Avalanche-size distributions for the values of disorder $R = 0.48, 0.50, 0.52, 0.54$. Main panel: Collapsing of the curves from the upper right inset according to Eq. (7) with the values of parameters and exponents $R_c = 0.31$, $\sigma = 0.11$ and $\tau + \sigma\beta\delta = 2.06$. Upper left inset: Collapsing of the integrated avalanche-size curves for the same disorders. (b) Inset: Avalanche-size distributions for the values of disorder $R = 0.42, 0.44, 0.46, 0.48, 0.50$. Main panel: Collapsing of the curves from the inset according to Eq. (7) with the values of parameters and exponents $R_c = 0.20$, $\sigma = 0.045$ and $\tau + \sigma\beta\delta = 2.06$.

impossible, in the upper right inset of Fig. 6(a) we show the distributions of avalanche sizes,

$$D_R^{(S,\mathrm{wnd})}(S) \equiv \int_{H_c^{\mathrm{eff}}(R)-r^{\beta\delta}h_0'}^{H_c^{\mathrm{eff}}(R)+r^{\beta\delta}h_0'} D_{R,H}^{(S)}(S)dH, \tag{8}$$

collected in the small windows of the external field for various disorders between $R = 0.48$ and $R = 0.54$. For each R the corresponding window is centered at the effective critical field $H_c^{\mathrm{eff}}(R)$, i.e., at the value of H at which the susceptibility $\chi_R(H)$ attains its maximum for that disorder. The size of each window on H axis is determined by $r^{\beta\delta}h_0'$, where the value of h_0' is chosen so that the windows are reasonably small still containing not too few avalanches in each run. As elaborated in Ref. [25], such windowed distributions should collapse according to Eq. (7), $D_R^{(S,\mathrm{wnd})}(S) = S^{-(\tau+\sigma\beta\delta)}\mathcal{D}_+^{(S,\mathrm{wnd})}(S^{\sigma}r)$, and their collapsing is shown in the main panel of Fig. 6(a), with the best values of collapsing parameters and exponents $R_c = 0.31 \pm 0.01$, $\sigma = 0.11 \pm 0.01$ and $\tau + \sigma\beta\delta = 2.06 \pm 0.05$. For the same set of values, in the upper left inset of Fig. 6(a) we show the collapsing of integrated avalanche-size distributions for the same disorders according to Eq. (7).

If we add curves for systems of lower disorders and try to collapse them for the same values of parameters and exponents we fail. To collapse those curves we have to shift the above presented values of parameters and exponents. In the main panel of Fig. 6(b) is presented how the curves collapse in the range of disorders from $R = 0.42$ to $R = 0.50$. The best collapse is obtained for the values $R_c = 0.20 \pm 0.01$, $\sigma = 0.045 \pm 0.001$ and $\tau + \sigma\beta\delta = 2.06 \pm 0.05$. This indicates that the value of the supposed critical disorder is significantly smaller than the lower one obtained above, i.e., 0.20, or that it even tends to zero. To further test the value of R_c by the presented method of curve collapsing one would need to include the curves corresponding to disorders even smaller than 0.42. This would demand a significant increase in the system size and number of simulations for different random-field configurations, which would eventually lead to an extreme increase of simulation time.

2. Avalanche-duration distributions

Similarly to the avalanche-size distribution, there is a scaling form [24,25]

$$D_{R,H}^{(T)}(T) = T^{-\alpha}\mathcal{D}_+^{(T)}(T^{\sigma\gamma}r, h'r^{-\beta\delta}), \tag{9}$$

for the distribution $D_{R,H}^{(T)}(T)$ of duration T of avalanches triggered at the value H of the external field in infinite system. Here, α is the duration distribution exponent, γ is the exponent describing the scaling $\langle T\rangle_S \sim S^{1/\gamma}$ of the mean duration $\langle T\rangle_S$ of avalanches having size S, while $\mathcal{D}_+^{(T)}$ is the universal scaling function for the avalanche-duration distribution $D_{R,H}^{(T)}(T)$ for disorders above the critical disorder R_c. Further, the integrated avalanche-duration distribution $D_R^{(T,\mathrm{int})}(T) \equiv \int_{-\infty}^{\infty} D_{R,H}^{(T)}(T)dH$ scales as

$$D_R^{(T,\mathrm{int})}(T) = T^{-(\alpha+\sigma\beta\delta\gamma)}\hat{\mathcal{D}}_+^{(T,\mathrm{int})}(T^{\sigma\gamma}r), \tag{10}$$

where $\hat{\mathcal{D}}_+^{(T,\mathrm{int})}(X) \equiv \int_{-\infty}^{\infty}\mathcal{D}_+^{(T)}(X,Y)dY$ is the universal scaling function for the integrated duration distribution $D_R^{(T,\mathrm{int})}(T)$. Finally, the corresponding duration distributions pertaining to finite systems approximately follow scaling Eqs. (9) and (10) provided their lattice size is sufficiently large.

Like for avalanche-size distributions, in the upper right inset of Fig. 7(a) we present the windowed avalanche-duration distributions $D_R^{(T,\mathrm{wnd})}(T) \equiv \int_{H_c^{\mathrm{eff}}(R)-r^{\beta\delta}h_0'}^{H_c^{\mathrm{eff}}(R)+r^{\beta\delta}h_0'} D_{R,H}^{(T)}(T)dH$. In the main panel of Fig. 7(a) we show a collapsing of the windowed size distributions obtained with the aid of $D_R^{(T,\mathrm{wnd})}(T) = T^{-(\alpha+\sigma\beta\delta\gamma)}\hat{\mathcal{D}}_+^{(T,\mathrm{wnd})}(T^{\sigma\gamma})$ with parameters' and exponents' values for the best collapse $R_c = 0.31 \pm 0.01$, $\sigma\gamma = 0.19 \pm 0.02$, and $\alpha + \sigma\beta\delta\gamma = 2.80 \pm 0.06$. In the upper left inset is given the collapse of integrated avalanche-duration distributions for the same systems and the same values of parameters and exponents.

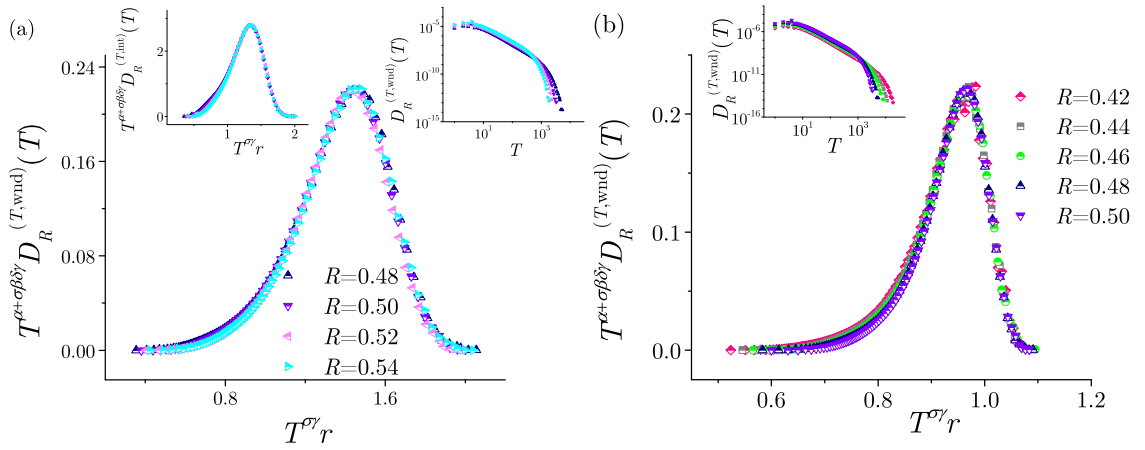

FIG. 7. (a) Upper right inset: Avalanche-duration distributions for the values of disorder $R = 0.48, 0.50, 0.52, 0.54$. Main panel: Collapsing of the curves from the upper right inset according to (10) with the values of parameters and exponents $R_c = 0.31$, $\sigma\gamma = 0.19$, and $\alpha + \sigma\beta\delta\gamma = 2.8$. Upper left inset: Collapsing of the integrated avalanche-duration curves for the same disorders. (b) Inset: Avalanche-duration distributions for the values of disorder $R = 0.42, 0.44, 0.46, 0.48, 0.50$. Main panel: Collapsing of the curves from the inset according to (10) with the values of parameters and exponents $R_c = 0.20$, $\sigma\gamma = 0.073$, and $\alpha + \sigma\beta\delta = 2.8$.

Similarly to the case of avalanche-size distribution, it becomes impossible to obtain a proper collapse of the avalanche-duration distribution curves with the above mentioned values of parameters and exponents if we add curves for systems with lower disorders. In the main panel of Fig. 7(b) we present a collapse of the avalanche-duration distribution curves for disorders that range from $R = 0.42$ to $R = 0.50$. Appropriate parameters and exponents read $R_c = 0.20 \pm 0.01$, $\sigma\gamma = 0.073 \pm 0.004$, and $\alpha + \sigma\beta\delta\gamma = 2.80 \pm 0.06$. The data presented in Fig. 7 are from the same set of simulations as the data shown in Fig. 6.

Again, as for the avalanche-size distributions, we see that as we try to collapse the distributions obtained for lower disorders the supposed value of critical disorder lowers as well. This indicates that either R_c is much smaller than 0.20, or that there is no nontrivial critical behavior for the athermal nonequilibrium RFIM on the hexagonal lattice.

As explained above, the simulation time would explode if we try to investigate larger systems with smaller disorders to obtain R_c via the method of curve collapsing. Additionally, if $R_c = 0$ then all previously mentioned collapsing procedures cannot be applied and some other investigation is needed to come closer to the answer. We want to see what happens in thermodynamic limit, but obviously, we are not able to simulate infinite systems. To this end we try to set some conditions in the system, before the evolution starts, that would mimic the behavior in the thermodynamic limit. This is presented in the next section.

In contrast to the hexagonal lattice, for the square and triangular two-dimensional lattices the parameters for which the best collapses of the distribution curves are obtained are stable regardless the disorder range. This is presented in Fig. 8(a) for square lattice of size $32\,768 \times 32\,768$ and disorders that range from $R = 0.68$ up to $R = 0.88$, and in Fig. 8(b) for triangular lattice of size $65\,536 \times 65\,536$ for disorders from $R = 1.09$ to $R = 1.30$. On the main panels of Fig. 8 are presented the appropriate collapses of avalanche-size distribution curves, while in insets are presented the collapses of avalanche-duration distribution curves. The values of parameters and exponents for which the best collapses are obtained are presented in Ref. [25] for square and in Ref. [41] for triangular lattice. This comparison shows the obvious difference between square and triangular lattices on one side and the hexagonal lattice on the other side. One possible reason for this difference might lie in the absence of the nontrivial critical behavior in the case of hexagonal lattice.

IV. SYSTEMS WITH PRESET INTERFACE

Since we saw that the linear decrease of H_c^{eff} versus R originates in finite-size effects we would like to eliminate them. That we intend by fixing one spin pointing upwards in the beginning and preventing it to change during the subsequent system evolution. That spin plays the role of the one that would be flipped if the system was large enough. Since the boundary conditions are closed it is irrelevant which spin we choose to flip. However, some problems arose if none of its three neighbors are able to start an avalanche before the external field is greater than some value at which a spanning avalanche occurs. This again leads to similar behavior as presented in Fig. 5. For this reason we fix in the beginning more than one spin pointing upwards. This gave more stable results, but there is a question whether we disturbed the system evolution if we fixed more than one spin pointing upwards. This is why we performed simulations with various preset interfaces, ranging from one spin up to whole linear size, i.e., L spins (in the system of size $L \times L$). If we take into account only those cases when no finite-size effects occur it turned out that the systems evolve independently on the preset interface length (from one to L), i.e., the systems behave in the same manner and all results presented in this section are the same irrespective of the number of preset spins. This allowed us to analyze the systems where the probability of seeing finite-size effects, in the sense of jumping to the non realistically values of external field, is the smallest. Those are the systems whose interface length is L. In those systems in all our simulation we didn't notice any finite-size effect, in the mentioned sense. By the preset interface of length l (in the system of size $L \times L$,

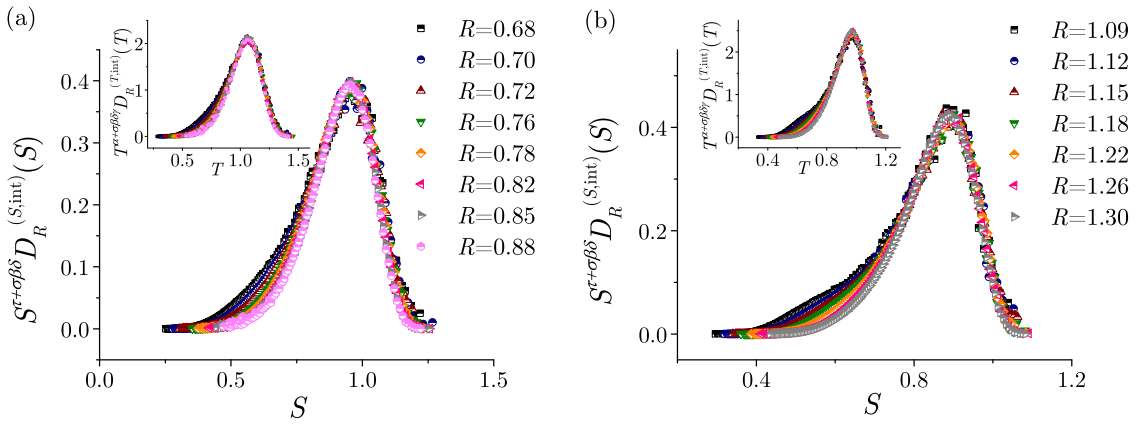

FIG. 8. (a) Main panel: Collapsing of the integrated avalanche-size distribution curves for the square lattice of size 32 768 × 32 768 according to Eq. (7) for the disorders that range from $R = 0.68$ to $R = 0.88$. Inset: Collapsing of the integrated avalanche-duration distribution curves according to Eq. (10) for the same data as in main panel. (b) Main panel: Collapsing of the integrated avalanche-size distribution curves for the triangular lattice of size 65 536 × 65 536 according to Eq. (7) for the disorders that range from $R = 1.09$ to $R = 1.30$. Inset: Collapsing of the integrated avalanche-duration distribution curves according to Eq. (10) for the same data as in main panel.

where $L \geqslant l$) we mean the line of l neighboring spins in one column whose orientations are set to $+1$ in the beginning of the simulation and are prevented from changing during the simulation.

A. Effective critical field

Let us start from the problem of dependence of effective critical field on system's disorder presented in Fig. 3(b) and Fig. 5. We repeated the same set of simulations for the systems with preset interface as we did with regular systems. In the main panel of Fig. 9 are presented the effective critical

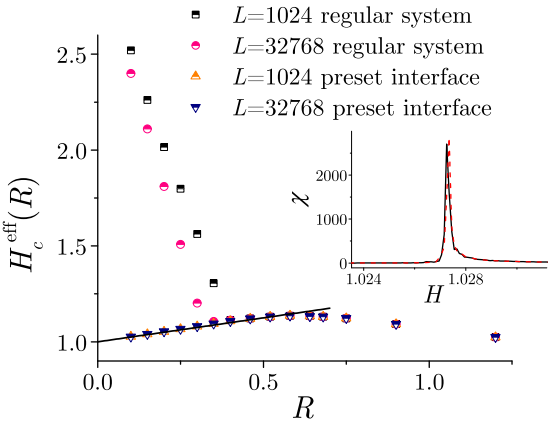

FIG. 9. Main panel: Effective critical field versus system's disorder R for regular systems and the systems with preset interface. Black squares represent regular systems of linear size $L = 1024$, pink circles represent regular systems of linear size $L = 32\,768$, orange triangles represent the systems with preset interface of linear size $L = 1024$, and blue inverted triangles represent the systems with preset interface of linear size $L = 32\,768$. Solid line shows the connection between effective critical field and disorder given by $p(-1) = 0.6$. Inset: Example of two single-run susceptibility curves, presented by black solid and red dashed lines, for system with preset interface and size 32 768 × 32 768 and disorder $R = 0.1$.

fields for the systems with preset interface for $L = 1024$ and $L = 32\,768$. For the sake of comparison there are also left the effective critical fields for the regular systems of the same sizes. We see that $H_c^{\text{eff}}(R)$ does not depend on L for the systems with a preset interface, meaning that we may take those values as the values of effective critical fields in the thermodynamic limit.

In a next step, let us notice the values of the effective critical field, obtained for disorders $R > R_c^{\text{eff}}$ are the same for regular systems and the systems with the preset interface. This is expected since above the effective critical disorder there are a lot of spins that may be flipped even if they are not connected to the interface, creating thus islands of flipped spins that dominantly determine the further system evolution.

An interesting result is that H_c^{eff} depends on R linearly even for the systems with the preset interface. But here, the slope is positive and is determined by the condition $p(-1) = 0.6$. So, for any system size and any disorder (up to $R \approx 0.5$) the susceptibility will reach the maximum once the external field is such that the flipping probability of a spin with exactly one flipped neighbor is approximately 0.6. Although at present we don't have any exact answer to the question why is that so we will try to give some clue in the next section on the avalanche propagation. In inset of Fig. 9 are presented two single-run susceptibility curves for the system with preset interface, size 32 768 × 32 768, and disorder $R = 0.1$. We see that even for that low disorder there are very little differences in the sample to sample comparison, which reminds on the situation from Fig. 3(a) for disorders above the effective critical disorder.

In Fig. 10(a) we present the analogous graphs for the square lattices and in Fig. 10(b) for the triangular lattices. There we notice that the values of $H_c^{\text{eff}}(R)$ differ for the various interface sizes for the disorders that are below the critical disorder. This suggests that there appears a difference in the values of $H_c^{\text{eff}}(R)$ for various preset interface sizes if the system is in ferromagnetic phase, while in the paramagnetic phase the values of $H_c^{\text{eff}}(R)$ remain the same no matter what is the size of the preset interface. Judging on this, it turns out

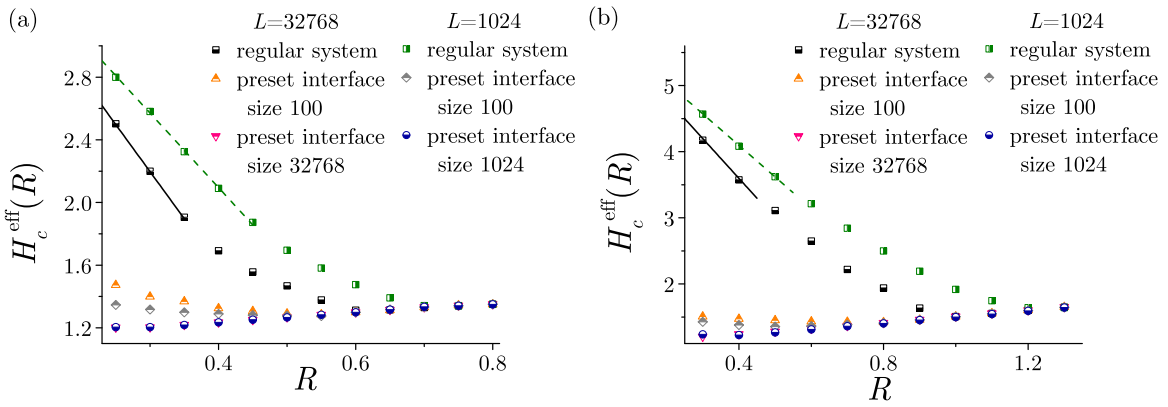

FIG. 10. (a) Effective critical field for the square lattice of the different sizes, $L = 1024$ and $L = 32\,768$, and for different preset interface values, zero interface (regular system), interface of size 100 and interface of the size of L. Straight lines represent fits obtained from Eq. (11). (b) The same as in (a) but for triangular lattice. Straight lines are obtained using Eq. (12).

that the two-dimensional hexagonal lattice is in paramagnetic phase for all disorders greater than zero.

Straight lines in Fig. 10 represent the theoretical predictions, that originates in finite-size effects, similar to Eq. (5), but for the square and triangular lattices. The methodology of deriving these predictions is the same, the only thing that differs is the number of nearest neighbors of the first flipping spin in the system. Thus, for the square lattice it reads

$$H_c^{\rm eff}(R) = 4 - R\sqrt{2}\,{\rm erf}^{-1}\left(1 - \frac{2}{L^2}\right), \tag{11}$$

and for triangular

$$H_c^{\rm eff}(R) = 6 - R\sqrt{2}\,{\rm erf}^{-1}\left(1 - \frac{2}{L^2}\right). \tag{12}$$

B. Spanning avalanches

Let us take a look at the appearance of spanning avalanches in the systems. We mentioned earlier that those avalanches play the role of infinite avalanches causing jump in magnetization of the infinite systems (i.e., in the thermodynamic limit). If there are no spanning avalanches in finite systems, then we may expect that there is no nontrivial critical behavior of the model.

In the main panel of Fig. 11 we show the average size of spanning avalanches over system size, $\langle S_{\rm sp\ av}\rangle/L^2$, for different disorders. The trend is decreasing. As the system size grows, the biggest avalanche in the system occupies less portion of the whole system. We see that for each system size there is a plateau of $\langle S_{\rm sp\ av}\rangle/L^2$ values, starting from $R = 0$ up to the $R = R_c^{\rm eff}(L)$. If there is no spanning (infinite) avalanche in the system in thermodynamic limit then we would expect that the plateau value tends to zero, i.e., $\lim_{L\to\infty}\langle S_{\rm sp\ av\ plateau}\rangle/L^2 = 0$. Thus, we propose a scaling of the plateau values as

$$\langle S_{\rm sp\ av\ plateau}\rangle/L^2 = \frac{a}{L^b}. \tag{13}$$

This relation would imply indeed that the plateau value goes to zero as the system grows. We tested it and in inset of Fig. 11 we present the proposed fit. We see that there is a good agreement between the fitting line and the numerical data for the parameters' values $a = 0.470 \pm 0.015$ and $b = 0.090 \pm 0.005$.

V. CLOSER INSIGHT TO THE AVALANCHE PROPAGATION

In this section we present some results that could be of interest for further study of avalanche propagation. Obviously, it is quite hard to give any kind of theoretical analysis for local avalanche propagation in such random systems. For this reason we were observing smaller systems, so that it is easier to track down the changes, with varying model parameters and try to "catch" some regularities in the evolution of those systems.

A. Avalanche propagation for a given value of external field

In the previous section we showed that there is a specific condition for appearing of the biggest avalanches which holds in a wide range of disorders starting from zero up to

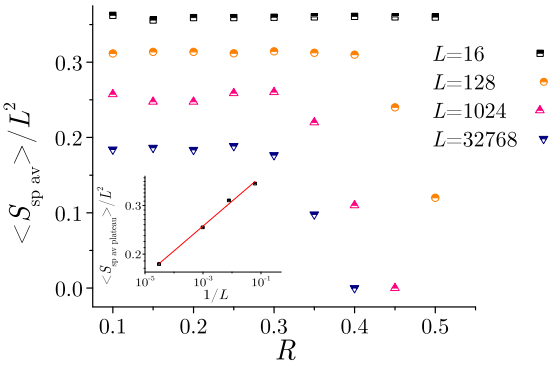

FIG. 11. Main panel: Fractional average size of spanning avalanche to the system size, $\langle S_{\rm sp\ av}\rangle/L^2$, versus disorder R. Black squares represent the systems of linear size $L = 16$, orange circles represent the systems of linear size $L = 128$, pink triangles represent the systems of linear size $L = 1024$, blue inverted triangles represent the systems of linear size $L = 32\,768$. Inset: The plateau values of fractional average size of spanning avalanche versus system size, fitted using Eq. (13).

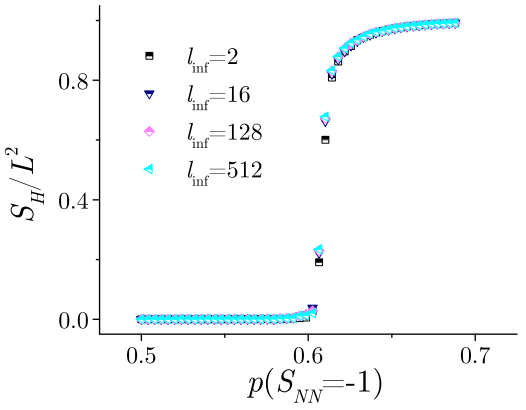

FIG. 12. Fractional size of avalanche, S_H/L^2, for a given value of external field [presented on x axis in terms of probability $p(-1)$]. The linear system size is $L = 1024$ and interface length $l_{\text{inf}} = 2, 16, 128, 512$. The disorder in all presented cases is $R = 0.1$.

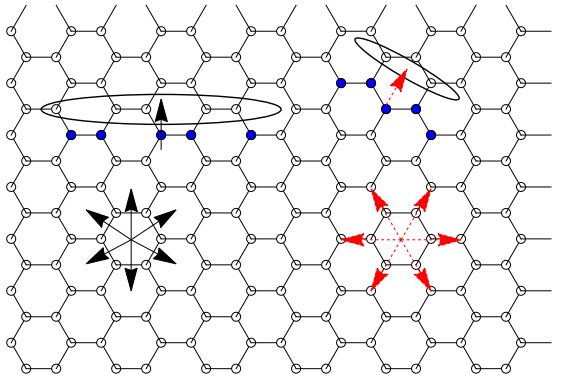

FIG. 13. Left lower: favorable avalanche propagation directions. Left upper: an example of the next step in propagation along the favorable direction. Right lower: nonfavorable avalanche propagation directions. Right upper: an example of the next step in propagation along the nonfavorable direction.

approximately 0.5. This condition reads that the probability of flipping a spin with exactly one flipped neighbor should be $p(-1) \approx 0.6$ independently on the system size. To closer investigate this rather interesting finding we simulated systems at a fixed value of external field with various preset interfaces. This gives us a clue whether there is a role of interface size or is it just the value of external field that dictates the avalanche propagation. The employed values of external field are such that the probability $p(-1)$ ranges from 0.5 up to 0.7. In the beginning the system is set in a way that the interface is flipped and all the nearest neighbors are active spins, i.e., if any of the interface neighboring spins is unstable, then it will flip and further avalanche propagation runs, as described in Sec. II. In this way we mimic the situation when the avalanche starts to propagate at a given value of external field and reaches some length of the front interface.

In Fig. 12 we show the impact of interface length on avalanche size. The system size is $L = 1024$, disorder $R = 0.1$, and the interface length takes values $l_{\text{inf}} = 2, 16, 128, 512$. We see that there are differences in avalanche size at a given external field only in the small range of growing part of the curve (just above the value 0.6 on x axis), where S_H/L^2 is larger for larger values of interface length. This is due to the larger probability of stopping an avalanche with a smaller interface length before it manages to create a larger propagation front, which is expected. Nevertheless, no matter what the value of interface length is, the avalanche size starts to grow at the same value of external field when $p(-1) \approx 0.6$.

The results presented in this subsection are the same regardless the value of disorder. We checked it for disorders from $R = 0.05$ up to $R = 0.45$, and the results coincide.

B. Stopping islands

Here we give a rather naive, but hopefully useful, explanation of what is the most efficient way of stopping an avalanche at the hexagonal lattice. In Fig. 13, black solid arrows (lower left part) present the directions along which the avalanche propagation is easier, while red dashed arrows (lower right part) show the directions along which the avalanches propagate hardly. To demonstrate that, we show the examples of necessary conditions to stop an avalanche. In the upper left part of Fig. 13 is presented one example of avalanche propagation along a favorable direction. To stop this avalanche all circled spins must not flip in the next moment of discrete time. If some of them flip, then their neighbors will flip almost surely (because they will have two flipped neighbors), prolonging even more the avalanche propagation. On the other side, in the upper right part of Fig. 13 is presented the avalanche propagation along one of the nonfavorable directions. We see that in this case the avalanche can be stopped only by not flipping every second spin in a row. This means that the avalanche will not propagate further even if it encounters an obstacle created from the nonconnected spins. It is easier to find such an obstacle than the one from the upper left part of Fig. 13 where the nonflipping spins are connected. That is why the avalanches propagate dominantly along the favorable directions.

In Fig. 14 is shown the system of size 16×16 whose disorder is $R = 0.1$. This is a state of that system when the external field is $H = 1.025$, i.e., $p(-1) = 0.598706$. Blue squares represent flipped spins, while circles represent the spins that are not flipped so far. Red circles represent the spins that do not flip with the given external field and have one flipped neighbor. On the other side, white circles are spins that would flip with given external field and with one flipped neighbor, but so far none of their neighbors is flipped, so they remain unflipped. As one can see, the most of the "edges" that stop the further avalanche propagation are along the nonfavorable directions for avalanche propagation.

In the case of square and (especially) triangular lattice the obstacles for avalanche propagation cannot be formed that easily. Namely, in those lattices avalanche can propagate in layers. Imagine an interface of flipped spins along a straight line in a square or triangular lattice. All spins in a layer next to the interface are connected between themselves, contrary to the hexagonal lattice. It is enough for one spin, connected

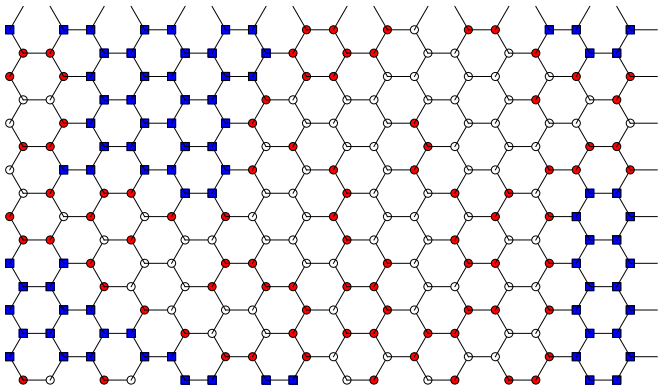

FIG. 14. System of size 16×16 and disorder $R = 0.1$ at external field $H = 1.025$. Blue squares are flipped spins. White circles are nonflipped spins that would flip if they had at least one flipped neighbor. Red spins are nonflipped spins that wouldn't flip even if they had one flipped neighbor.

to the interface, to flip, and after that its neighbor will have two flipped neighbors, which will, very probably (because its effective field is changed by 2), force that spin to flip, forcing further its neighbor to flip...and so on until the whole layer is flipped. The same mechanism repeats for the next layer, which in combination with the already flipped isolated islands of spins in the system creates a spanning avalanche. As mentioned, such a mechanism is not possible in the hexagonal lattice, since the geometry does not allow that the spins which are neighbors of the interface of flipped spins belong to the one connected layer.

VI. DISCUSSION AND CONCLUSION

Our results, presented in the previous sections, provide a numerical evidence that there is no nontrivial critical behavior of the nonequilibrium athermal random-field Ising model on the hexagonal 2D lattice. This is corroborated by the variation of the critical parameters and exponents for collapses of avalanche parameters distributions for different ranges of disorders and by the results obtained from simulations of systems with the preset interfaces collected from extensive simulations that were performed in a wide range of disorders and on the systems containing up to $\approx 10^9$ spins. We also gave a closer insight to the avalanche propagation in the last section. Several other manifestations of model's criticality (like the correlation functions, joint distributions, distributions of avalanche energy and amplitude, and distributions of moments) we have omitted here for the purpose of simplicity concentrating only on the most important distributions of avalanche size and duration.

The foregoing statements support the conclusions stated in Refs. [38,39,49], although the models analyzed in these papers are somewhat different from ours. Also, we inspected here much larger lattices to try to avoid the finite-size effects as much as possible. For the analysis of cases when even the biggest lattices were not large enough we introduced a method for investigation of criticality, utilizing the preset interface, that mimic the behavior in thermodynamic limit. By this method we discovered that for a range of disorders from zero up to ≈ 0.5 the value of the external field for which the susceptibility reaches the maximum is determined by the condition that the probability of flipping a spin whose exactly one neighbor is flipped is $p(-1) \approx 0.6$. This result might be interesting for future theoretical analysis of the RFIM on hexagonal lattice.

Until recently, it was commonly considered that the variants of the nonequilibrium athermal RFIM situated on lattices of the same dimensionality should belong to the same universality class despite the possible differences in lattice topologies (e.g., number of nearest neighbors and their interconnections). However, this standpoint was challenged in Refs. [38,39] by the conjecture that "the existence of critical hysteresis depends on the coordination number of the lattice rather than the dimensionality of space in which the lattice is embedded"; see Ref. [39]. Our present numerical analysis, together with the results of previous numerical studies [24,41], makes this conjecture questionable by indicating that the lattice topology in regular 2D lattices can influence not only the nonuniversal critical parameters and critical exponents, but also the existence of a nontrivial critical behavior.

The results on different lattices in two dimensions presented in papers [24,38,39,41] and in the present one can be compared. These works deal with the question of the critical behavior of the nonequilibrium RFIM on triangular, square and hexagonal two-dimensional lattices. For the square and triangular lattices there are differences in the values of critical parameters and critical exponents. Still, they follow the same collapsing procedures of distributions of avalanche parameters and obey the same rules regarding the collapsing of the magnetization and susceptibility curves. Those are the rules presented by Eqs. (7) and (10) and analogous laws for other quantities in Ref. [25]. However, one could raise a question what if those collapses fail as they do in the case of hexagonal lattice, which is presented here in Sec. III. The collapsing works in the vicinity of critical point. Thus, the curves that were obtained for the systems whose disorders are not much above the critical disorder should collapse for the same set of critical exponents and parameters no matter what range of disorders is in question. This is the case in Refs. [24,41] for square and triangular lattices. But, as it can be seen, that is not the case for the hexagonal lattice. The change of range of disorders for curves that are collapsed leads to the relatively large change in estimated values of parameters and exponents. These results suggest that the critical disorder is significantly smaller than the the values used for data collapsing in two different ranges of disorder and that some other approaches are to be used to conclude further on the criticality of the RFIM on hexagonal lattice.

To conclude, in this paper we have presented the results of a numerical study of the nonequilibrium athermal random-field Ising model in adiabatic regime on the hexagonal 2D lattice. Our results, based on extensive simulations involving regular systems and systems with preset interface with up to $\approx 10^9$ spins, provide the evidence suggesting that this variant of model do not exhibits a nontrivial critical behavior. Previous results showed that the values of the exponents and nonuniversal critical parameters are different on the square and on the triangular 2D lattices. Together with the present result, this supports the recent conjecture that the number of nearest

neighbors, together with the lattice dimensionality, affect the model criticality not only in terms of the nonuniversal critical parameters and the values of the model exponents, but also altering the existence of nontrivial critical behavior.

ACKNOWLEDGMENT

This work was supported by the Ministry of Education, Science, and Technological Development of the Republic of Serbia.

[1] F. Omori, J. Coll. Sci., Imp. Univ. Tokyo **7**, 111 (1894).
[2] H. Kanamori and E. E Brodsky, Rep. Prog. Phys. **67**, 1429 (2004).
[3] E. A. Jagla, F. P. Landes, and A. Rosso, Phys. Rev. Lett. **112**, 174301 (2014).
[4] F. Lombardi, H. J. Herrmann, D. Plenz, and L. de Arcangelis, Sci. Rep. **6**, 24690 (2016).
[5] E. Vives, J. Ortín, L. Mañosa, I. Ràfols, R. Pérez-Magrané, and A. Planes, Phys. Rev. Lett. **72**, 1694 (1994).
[6] M. Bretz, J. B. Cunningham, P. L. Kurczynski, and F. Nori, Phys. Rev. Lett. **69**, 2431 (1992).
[7] D. S. Fisher, Phys. Rep. **301**, 113 (1998).
[8] J. P. Sethna, K. A. Dahmen, and O. Perković, in *The Science of Hysteresis*, edited by G. Bertotti and I. Mayergoyz (Academic Press, Amsterdam, 2006).
[9] K. A. Dahmen, J. P. Sethna, M. C. Kuntz, and O. Perković, J. Magn. Magn. Mater. **226**, 1287 (2001).
[10] G. Bertotti and M. Pasquale, J. App. Phys. **67**, 5255 (1990).
[11] S. Franz, G. Parisi, F. Ricci-Tersenghi, and T. Rizzo, Eur. Phys. J. E **34**, 102 (2011).
[12] E. Vives and A. Planes, Phys. Rev. B **50**, 3839 (1994).
[13] E. Vives and A. Planes, J. of Magn. and Magn. Mat. **221**, 164 (2000).
[14] D. P. Belanger and T. Nattermann, in *Spin Glasses and Random Fields*, edited by A. P. Young (World Scientific, Singapore, 1998).
[15] J. P. Sethna, K. A. Dahmen, S. Kartha, J. A. Krumhansl, B. W. Roberts, and J. D. Shore, Phys. Rev. Lett. **70**, 3347 (1993).
[16] G. Durin and S. Zapperi, in *The Science of Hysteresis*, Vol. 2, edited by G. Bertotti and I. Mayergoyz (Elsevier/Academic Press, Amsterdam, 2006), pp. 181–267.
[17] Dj. Spasojević, S. Bukvić, S. Milošević, and H. E. Stanley, Phys. Rev. E **54**, 2531 (1996).
[18] J. P. Sethna, K. A. Dahmen, and O. Perković, in *The Science of Hysteresis*, Vol. 2, edited by G. Bertotti and I. Mayergoyz (Elsevier/Academic Press, Amsterdam, 2006), pp. 107–179.
[19] Dj. Spasojević, S. Janićević, and M. Knežević, Europhys. Lett. **76**, 912 (2006).
[20] K. A. Dahmen and J. P. Sethna, Phys. Rev. Lett. **71**, 3222 (1993).
[21] K. A. Dahmen and J. P. Sethna, Phys. Rev. B **53**, 14872 (1996).
[22] O. Perković, K. A. Dahmen, and J. P. Sethna, Phys. Rev. Lett. **75**, 4528 (1995).
[23] O. Perković, K. A. Dahmen, and J. P. Sethna, Phys. Rev. B **59**, 6106 (1999).
[24] Dj. Spasojević, S. Janićević, and M. Knežević, Phys. Rev. Lett. **106**, 175701 (2011).
[25] Dj. Spasojević, S. Janićević, and M. Knežević, Phys. Rev. E **84**, 051119 (2011).
[26] I. Balog, G. Tarjus, and M. Tissier, Phys. Rev. B **97**, 094204 (2018).
[27] L. X. Hayden, A. Raju, and J. P. Sethna, Phys. Rev. Res. **1**, 033060 (2019).
[28] N. G. Fytas and V. Martin-Mayor, Phys. Rev. Lett. **110**, 227201 (2013).
[29] N. G. Fytas, V. Martin-Mayor, M. Picco, and N. Sourlas, Phys. Rev. Lett. **116**, 227201 (2016).
[30] N. G. Fytas, V. Martin-Mayor, M. Picco, and N. Sourlas, Phys. Rev. E **95**, 042117 (2017).
[31] N. G. Fytas, V. Martin-Mayor, G. Parisi, M. Picco, and N. Sourlas, Phys. Rev. Lett. **122**, 240603 (2019).
[32] V. Navas-Portella and E. Vives, Phys. Rev. E **93**, 022129 (2016).
[33] Dj. Spasojević, S. Mijatović, V. Navas-Portella, and E. Vives, Phys. Rev. E **97**, 012109 (2018).
[34] B. Tadić, S. Mijatović, S. Janićević, Dj. Spasojević, and G. J. Rodgers, Sci. Rep. **9**, 6340 (2019).
[35] S. Mijatović, D. Jovković, S. Janićević, and Dj. Spasojević, Phys. Rev. E **100**, 032113 (2019).
[36] S. Mijatović, M. Branković, S. Graovac, and Dj. Spasojević, Phys. Rev. E **102**, 022124 (2020).
[37] D. Thongjaomayum and P. Shukla, Phys. Rev. E **88**, 042138 (2013)
[38] L. Kurbah, D. Thongjaomayum, and P. Shukla, Phys. Rev. E **91**, 012131 (2015).
[39] P. Shukla and D. Thongjaomayum, J. Phys. A: Math. Theor. **49**, 235001 (2016).
[40] D. Thongjaomayum and P. Shukla, Phys. Rev. E **99**, 062136 (2019).
[41] S. Janićević, S. Mijatović, and Dj. Spasojević, Phys. Rev. E **95**, 042131 (2017).
[42] O. Perković, K. A. Dahmen, and J. P. Sethna, arXiv:cond-mat/9609072.
[43] M. C. Kuntz, O. Perković, K. A. Dahmen, B. W. Roberts, and J. P. Sethna, Comput. Sci. Eng. **1**, 4 (1999).
[44] Dj. Spasojević, S. Janićević, and M. Knežević, Phys. Rev. E **89**, 012118 (2014).
[45] F. J. Pérez-Reche and E. Vives, Phys. Rev. B **67**, 134421 (2003).
[46] F. J. Pérez-Reche and E. Vives, Phys. Rev. B **70**, 214422 (2004).
[47] M. Schwartz and A. Soffer, Phys. Rev. Lett. **55**, 2499 (1985).
[48] N. G. Fytas and V. Martin-Mayor, Phys. Rev. E **93**, 063308 (2016).
[49] S. Sabhapandit, D. Dhar, and P. Shukla, Phys. Rev. Lett. **88**, 197202 (2002).